MAGNETIC RESONANCE IN MEDICINE **20**, 268–284 (1991)

Temporal and Spatial Analysis of Fields Generated by Eddy Currents in Superconducting Magnets: Optimization of Corrections and Quantitative Characterization of Magnet/Gradient Systems[1]

CH. BOESCH,[2] R. GRUETTER,[3] AND E. MARTIN

University Children's Hospital, Zürich, Switzerland

Received January 30, 1990; revised July 31, 1990

We propose methods for the spatial and temporal characterization of time-dependent magnetic fields generated by eddy currents after switching gradients. For an on-line determination of the temporal variations of the fields, we extract two terms from the unresolved signal of an extended sample, describing the time evolution of a frequency shift $\gamma\Delta B_z(t)$ and of a decay constant $k(t)$. This procedure allows us to optimize interactively the multiexponential pre-emphasis as well as any spectral volume selection method with respect to eddy currents. Additionally, we suggest an imaging sequence which allows us to determine the spatial distribution of eddy current fields at a chosen time-point after any gradient sequence to be tested. Expansion of these eddy currents fields into spherical harmonic functions proves the existence of a higher order terms, which cannot be corrected by a standard pre-emphasis device, where time constants and amplitudes are adjusted on the X, Y, Z, and $Z0$ coils. The proposed numerical analysis gives a tool to characterize any magnet/gradient system quantitatively with respect to eddy current performance.

INTRODUCTION

Temporally and spatially changing magnetic fields are used for magnetic resonance imaging as well as for some spectroscopic localization methods. According to Faraday's law, these "gradient pulses" induce currents in conducting structures (*1, 2*) such as probe head (antenna), shim/gradient coils, room-temperature tube, cooling shields, dewar walls, isolation, superconducting correction coils, and the main coil. The induced eddy currents create opposing magnetic fields (Lenz' law), thus always reducing the effect of the switching current in the gradient coils. Depending on the degree of interaction in a real magnet, these eddy currents can reduce the amplitude of a switched gradient up to 50% within the first milliseconds. The effects of the eddy currents depend strongly on the material of the conducting structures and persist from several milliseconds up to seconds.

There are two principal strategies to handle eddy current problems:

[1] Presented in part at the 8th Annual Meeting of the Society Magnetic Resonance in Medicine, Amsterdam, Proceedings Vol. 2, p. 967, Soc. Magn. Reson. Med., Berkeley, 1989.

[2] Present address: MR-Center, University and Inselspital, Inselheimmatte, CH-3010 Bern/Switzerland.

[3] Present address: Yale University, MR-Center, 333 Cedar Street, PO Box 3333, New Haven, CT 06510.

0740-3194/91 $3.00

(A) Reduce the generation of the currents by increasing the distance between gradient coils and surrounding conducting structures, by active shields (*3*) or by magnet technology.

(B) Correct the effect of the currents by additional currents in the gradient coils ("pre-emphasis").

In this article, we present methods for the determination of time-dependent magnetic fields produced by eddy currents after gradient switching. These methods allow an interactive optimization and a quantitative characterization of a magnet/gradient system. The application of the quantitative analysis to an existing MR magnet proves that significant amplitudes of higher order gradients are induced which cannot be corrected completely by any feasible pre-emphasis unit.

Most strategies for the adjustment of the pre-emphasis are based on the observation of a series of FIDs after gradient switching using a large sphere or several microscopic probes. Multiple microprobes show frequency shifts only, whereas an extended volume in a real, always slightly asymmetric magnet experiences all terms of the temporal inhomogeneity, i.e., B_0 shifts, as well as gradients. This results in a dephased signal with a short T_2^*. From the spatially unresolved signal of an extended volume, we extracted a frequency shift $\gamma \Delta B_z(t)$ and a decay constant $k(t)$, both time-dependent. This rapid method permits an interactive adjustment of the pre-emphasis compensation unit as well as an optimization of spectral localization techniques with respect to eddy currents. The effect of added "dummy" gradient pre-pulses for a minimization of eddy current effects from an ISIS pulse sequence (*4*) is demonstrated.

Additionally, we introduce an imaging sequence that allows to determine the spatial dependence of magnetic fields due to eddy currents generated by any gradient switching sequence. From these field maps the available volume for the acquisition of resolved spectra can be defined. A mathematical analysis of the obtained field maps allows a quantitative characterization of a real magnet/gradient system. An application on an existing high-field/small-bore system shows the presence of highly nonlinear terms in the induced magnetic fields which can obviously not be corrected by a standard pre-emphasis device, where time constants and amplitudes are adjusted on the X, Y, Z, and $Z0$ coils. Thereby, it is unavoidable to reduce eddy current effects as much as possible by means of increased spatial distances, active shielded gradients, or magnet technology.

The proposed characterization of residual eddy current fields may help the theoretical understanding of magnets and gradient systems. It also allows the optimization of an already installed magnet and the design of eddy current-insensitive pulse sequences.

MATERIALS AND METHODS

MR-System and Materials

All experiments were performed on a 2.35-T magnet (MEDSPEC 24/40, Bruker–Spectrospin, Fällanden Switzerland) with a room temperature bore of 40 cm (*5*). The gradient/shim set of this magnet is unshielded and consists of 15 independent coils: z_0 (used for B_0 pre-emphasis), linear x, y, z (used for gradients and linear pre-emphasis), and 11 higher order coils for shimming. The maximum gradient strength is

approximately 10 mT/m. The gradient system has an inner diameter of 35 cm and fits tightly into the room temperature bore (40 cm) of the magnet. First observations of nonlinearities of our gradient system were reported recently (*6*).

The pre-emphasis unit corrects the influence of each gradient on B_0 with three exponential functions (one amplitude and one time-constant each). Currents in the gradient coils are corrected for the influence of the very same gradient (not for crossed influences) with three exponential functions. Thus, the adjustment of the pre-emphasis unit includes the optimization of 36 parameters.

A 12-cm-diameter glass sphere filled with distilled water served as source of the signals.

Description of the Analysis of the FID

In the absence of an irradiating field B_1, the Bloch-equations in the *rotating frame* can be written as

$$\dot{M}_x = \gamma M_y \Delta B_z - kM_x \quad [1]$$

$$\dot{M}_y = -\gamma M_x \Delta B_z - kM_y, \quad [2]$$

with $k = 1/T_2$ and M_x, M_y, $\dot{M}_x$, and $\dot{M}_y$ = magnetization components and its time derivatives.

From [1] and [2], the offset frequency $\gamma \Delta B_z$ and the decay constant k can be extracted from the FID at any time, which allows us to consider $\gamma \Delta B_z(t)$ and $k(t)$ as time-dependent,

$$\gamma \Delta B_z(t) = \frac{\dot{M}_x M_y - \dot{M}_y M_x}{M_x^2 + M_y^2} \quad [3]$$

$$k(t) = -\frac{\dot{M}_x M_x + \dot{M}_y M_y}{M_x^2 + M_y^2}. \quad [4]$$

The term $\gamma \Delta B_z(t)$ permits an estimation of the time-dependent B_0 field shifts. Commonly, the dephasing of the FID due to static inhomogeneities is summarized in a time-independent $1/T_2^*$. In a similar way, we use $k(t)$ for an estimation of the time-dependent field inhomogeneity. Obviously, a direct interpretation of such derivatives of the Bloch equations is only possible in a sample with a single resonance frequency $\gamma \Delta B_z(t)$ and decay constant $k(t)$. Under Results, it is shown that nevertheless, this analysis gives enough information for an interactive improvement of the pre-emphasis when extended samples are used.

After detection and amplification, the real and imaginary part of the FID, $u(t)$ and $v(t)$, respectively, are proportional to the magnetization components M_x and M_y. In the present work, sequential sampling between the u and v channel is used (*7*). The digitization yields the two components u_i and v_i ($i = 0 \cdots 1/2$ memory size). With a constant sampling interval Δt for each channel, the components $u(t)$ and $v(t)$ and their time derivatives can be interpolated at a given time $t = i * \Delta t$ from the digitized values u_i and v_i.

$$M_x(t) \propto u(t) = u_i$$

$$M_y(t) \propto v(t) \approx \frac{v_i + v_{i-1}}{2}$$

$$\dot{M}_x(t) \propto \dot{u}(t) \approx \frac{u_{i+1} - u_{i-1}}{2\Delta t}$$

$$\dot{M}_y(t) \propto \dot{v}(t) \approx \frac{v_i - v_{i-1}}{\Delta t}. \qquad [5]$$

For simultaneous sampling, analogous expressions can be derived. Note that no arctan function has to be calculated which saves computer time and avoids phase discontinuities within a single FID. A second advantage of the above analysis is that the result does not depend on long-term fluctuations of the signal amplification, since the proportionality constant between magnetization and amplified signals in Eq. [5] cancels in Eqs. [3] and [4].

By the observation and analysis of a series of carefully shimmed FIDs, it is possible to follow time intervals of several seconds, although a single FID decays within a shorter time period. In the presented data of Fig. 1, eight consecutive FIDs, generated by pulses with very small flip angles (approximately 2°), are recorded with a freely selectable time interval after turning the gradients off. The small flip angles α of the excitation pulses ensure that the dominant source of the signal is the FID, since the amplitude of the echoes is proportional to $\sin \alpha * \sin^2(\alpha/2)$ ("primary" or "eight-

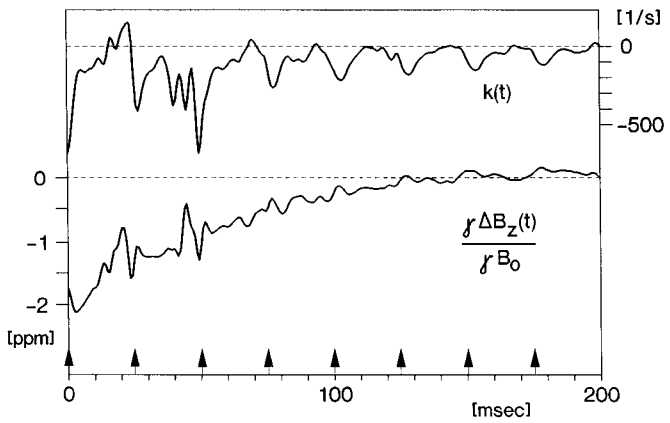

FIG. 1. Time-dependence of the offset frequency $\gamma\Delta B_z(t)$ (lower trace) and decay $k(t)$ (upper trace) 20 ms after 6 mT/m x gradient pulse of 2500 ms duration, estimated by an analysis of the FID according to Eqs. [3] and [4]. Eight FIDs (arrows indicate the timing of the rf pulses of approximately 2°) were acquired in a series to cover the whole time period of 200 ms. The decay analysis $k(t)$ (upper trace) shows the difference between two decays, one with and one without switched gradients. The pre-emphasis unit for the gradient x was carefully optimized prior to this experiment but required a compromise over a range of different gradient strengths, since the induced eddy currents are not a perfectly linear function of the x gradient amplitudes.

ball" echo) and to $\sin^3\alpha$ (stimulated echo), respectively. To reduce the detection of any residual xy magnetization during the subsequent acquisition, the repetition time of the pulses has to be longer than the FID. Due to the inherent lower signal-to-noise ratio, the calculation of $\gamma\Delta B_z(t)$ and $k(t)$ becomes less accurate toward the end of the FID, resulting in larger signal variations. If continuous recording is required, the repetition time between the pulses and the decay of the FID should be matched. For the interactive adjustment of the pre-emphasis unit, our usual practical approach was a fixed number of pulses and a variable waiting period between fixed acquisition times. Longer time periods (up to 4 s) were covered by longer waiting periods. Continuous recording was used at the end of the optimization procedure (Fig. 1). For the determination of the decay constant $k(t)$, reference data (baseline) are recorded without gradient switching and subtracted from each subsequent FID in order to compensate for the intrinsic T2* decay of the FID, thus extracting the effects of the additional gradients.

Description of the Imaging Sequence

To map the spatial variations of the eddy current fields, we used the imaging sequence presented in Fig. 2. It is based on a stimulated echo where the selective third pulse defines the slice. The first and second pulse are broad-banded (100 μs) and introduce minimal off-resonance effects. The slice gradient during the second pulse and the negative lobe of the read gradient are for trim purposes (rephasing). The eddy current field distribution generated by any gradient pulse train can be tested if it is placed

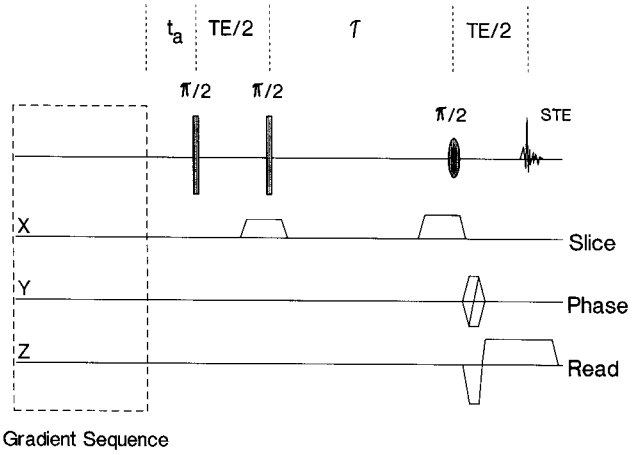

FIG. 2. The imaging pulse sequence used to measure time-dependent field shifts due to eddy currents created by any gradient switching sequence (dashed box). The sequence is applied twice, once with and once without a gradient sequence to be tested. The differences of the phase acquired during the first TE/2 is proportional to the time integral of the eddy current-related field strengths, provided the time interval τ is sufficiently long. In this article, a τ of approximately 1 s is used. The delay t_a is freely selectable and allows the acquisition of a series of images, showing the time evolution of the effects.

prior to this imaging sequence, as indicated by the dashed box in Fig. 2. The imaging sequence is repeated twice, once with the gradient sequence to be tested, once without. To reduce the influence of the switching gradient in the second TE/2 period for the majority of the eddy currents to a negligible degree, the time τ between pulse 2 and 3 of the stimulated echo is as long as possible (typically over a second). Any fluctuation of the magnetic field in a voxel during the first time period TE/2 causes thus a phase shift. Taking the difference of the phase images with and without the tested gradient sequence consequently reveals influences of magnetic field fluctuations due to the switching of the gradients. The formation of an image gives the spatial information, a series of different time intervals t_a between the gradient sequence and the start of the first pulse yields the time evolution of the field fluctuations. With the reasonable assumption that eddy currents act independent (i.e., that the presence or absence of a test sequence does not influence effects of the gradient switching of the imaging sequence), all influences of the gradients forming the imaging sequence are set to zero by the difference of the two phase images.

To avoid too many phase-discontinuities, the images without gradient switching were automatically phase corrected (zero and first order correction) by commercial software. The stored correction term was then used for the data acquisition after the gradient was switched on. Taking the difference of the two images subsequently cancelled this identical correction. For the quantitative analysis, different image pairs were normalized with respect to the magnetic center by subtracting the value in the center from all points in the image.

All imaging data presented in the text were obtained after careful adjustment of the pre-emphasis correction unit.

The data in the images represent phase differences which were acquired during the first echo interval TE/2. An average gradient field strength G during the time period TE/2 acquires a phase δ according to:

$$\delta/2\pi = \mathrm{TE}/2 * \nu = \mathrm{TE}/2 * \gamma/2\pi * G. \qquad [6]$$

Eq. [6] allows us to calculate an average gradient strength G during the time period TE/2 between the first two pulses of the stimulated echo in Fig. 2.

Determination of Inhomogeneities after Gradient Switching

The only difference between the data obtained by the imaging sequence in Fig. 1 and static inhomogeneities of a magnet lies in the transient character of the eddy current fields. In magnet technology, standard methods have been published to analyze static inhomogeneities (*8*) quantitatively. A field map, obtained with the imaging sequence of Fig. 2 at a fixed time t_a after gradient switching, represents a snapshot of time varying inhomogeneities, which can be analyzed by these standard methods (*8*). Throughout this paper, we have used a terminology adapted from (*8*). A magnetic field usually can be expressed as a sum of an orthogonal system of spherical harmonic functions (origin at the center of the magnet),

$$T_{nm} = A_{nm} r^n P_{nm}(\cos\theta)\sin(m\phi) \qquad [7]$$

$$T_{nm} = B_{nm} r^n P_{nm}(\cos\theta)\cos(m\phi). \qquad [8]$$

It is characteristic of these functions that they separate the terms containing the three parameters r, θ and ϕ. The term r^n describes the dependence of the magnetic field from the distance to the magnetic center. The associated Legendre functions $P_{nm}(x)$ (see table in (*8*)) contain only the angle θ and are independent of the radius r or the rotation around the z axis. This angular dependence of the magnetic field from the rotational angle around the z axis is described by the terms $\sin(m\phi)$ and $\cos(m\phi)$, which modulate the magnetic field on circles with the multiplicity of m. Functions with $m = 0$ represent a special case, the so-called "zonal" harmonics, with the Legendre functions $P_n(x)$.

$$T_n = C_n r^n P_n(\cos\theta). \qquad [9]$$

These zonal harmonics don't depend on the rotation angle around the z axis and can be written in a simple mathematical form for points on the z axis ("on-axis"). This allows an easy determination of the coefficients C_n in Eq. [9] by a polynomial regression of the magnetic field just on the z axis.

Another method is frequently used to determine the so-called "off-axis" coefficients A_{nm} and B_{nm} Eqs. [7] and [8] numerically: The magnetic field is measured at a discrete number of points on the surface of a cylinder or a sphere in the magnet (*8*), allowing the calculation of the coefficients in Eqs. [7] and [8]. The coefficients C_n in Eq. [9] could also be obtained by this method but with less accuracy than with the above mentioned "on-axis" determination.

Commonly, the main characteristics in the cartesian coordinate system are used for the notation of the different terms (see Table 1). This notation is familiar to spectroscopists because shim coils are built such that their spatial variation should correspond to one of the orthogonal spherical functions.

TABLE 1

Common Abbreviations for the Coefficients A_{nm}, B_{nm}, and C_n of the Spherical Harmonics (*8*) in Eqs. [7]–[9][a]

	m		
n	0	1	2
1	z	x	
		y	
2	z^2	xz	$x^2 - y^2$
		yz	xy
3	z^3	xz^2	$z(x^2 - y^2)$
		yz^2	zxy
4	z^4		

[a] The notation is chosen analogous to cartesian coordinates. Shown are only those which exist as shim coils in the MR system used (*5*).

For the data presented in Table 2A and 2B, we measured the field on a cylindrical surface in images obtained from a 12-cm sphere with the sequence of Fig. 2. The slices (in sagittal/coronal direction) were tilted in 22.5° steps around the z axis, thus allowing

TABLE 2

Determination of the Spherical Harmonics in Eqs. [7]–[9] Describing the Time-Dependent Magnetic Field[a]

(A) Values of the coefficients A_{nm}, B_{nm}, and C_n, respectively, in Hz/cm^n:

	m			
n	0	1	2	3
1	−2.78	10.33		
		1.03		
2	0.61	−0.15	0.15	
		−0.01	0.13	
3	0.02	−0.42	−0.00	0.00
		−0.00	−0.00	0.00
4	−0.00	0.00	0.00	0.00
		−0.00	0.00	0.00

(B) Maximum-values of the components of the field [in Hz] on a sphere of 8 cm radius[b]

	m			
n	0	1	2	3
1	−22.20	82.66		
		8.24		
2	38.81	−14.16	28.87	
		−0.59	24.66	
3	10.16	−438.90	−1.39	17.54
		−1.04	−7.77	10.09
4	−9.41	17.39	6.16	7.68
		−5.57	2.73	7.48

[a] Field inhomogeneities were determined 20 ms ($=t_a$) after a 3 mT/m x gradient pulse of 2500 ms duration. The echo period TE/2 was 15 ms. On-axis coefficients C_n ($m = 0$) were determined from the average of 9 series of 17 points measured along the z axis. Off-axis coefficients A_{nm} and B_{nm} were calculated from measurements on a cylindrical surface. The term with $n = 0$ and $m = 0$ represents the main field z_0 and is therefore not indicated. An average error of about 12% was estimated from the repetition of the experiment after several weeks.

[b] This volume is approximately covered by the head of a child. Note the increased influence of the terms with a higher value of n (e.g., A_{31}), which depend on r^n.

a measurement of the field in 22.5° steps around a series of 7 parallel circles, each on a plane perpendicular to the z axis. The circles with a radius of 3.4 cm had $z = -4.2$, -2.8, -1.4, 0, $+1.4$, $+2.8$, and $+4.2$ cm distance from the magnet center in the z direction. A transverse slice at $z = 0$ was used to test the reproducibility of the values on the innermost circle, serving as an internal control of the star-like arrangement of the images.

The "on-axis" components (C_n in Eq. [9]) were determined on the z axis in all tilted slices separately, using 17 points spaced by 0.7 cm.

It is important to note that the r^n dependence emphasizes terms of higher value of n at locations remote from the center of the magnet. To illustrate the influence of the individual components on the inhomogeneity, the maximal value on a sphere of 8-cm radius is given in Table 2B for each function. The position of the maxima is not necessarily identical for the different functions.

All data were obtained after careful adjustment of the pre-emphasis unit. To avoid any influence from induced currents in the other shim coils and from the electronics of the shim power supply, all shim coils (except x, y and z) have been physically disconnected.

RESULTS

Analysis of the FID after Gradient Switching

The proposed one-dimensional analysis of the FID (Eqs. [3] and [4]) yields a decay constant $k(t)$ and a frequency $\gamma \Delta B_z(t)$ on-line and has consequently been used for the manual optimization of the correction currents in the pre-emphasis unit. The calculation of the frequency shift $\gamma \Delta B_z(t)$ shows minor discontinuities at times when pulses are applied, whereas the decay analysis $k(t)$ reveals each FID as a hump (Fig. 1). Both curves are sensitive indicators for the time-dependent behavior of the magnetic field after gradient switching. This sensitivity is illustrated by Fig. 1, which was recorded *after* careful adjustment of the pre-emphasis unit. The remaining eddy current effects in Fig. 1 are clearly detected by the FID-analysis and present a compromise over the mostly used range of gradient strengths. In our magnet, a complete correction for all amplitudes of the x gradient is impossible since induced eddy currents are not a perfectly linear function of the x gradient strength. In Fig. 1, the stationary gradient (x) still disturbs the signal significantly within the first 200 ms after it has been switched off and shifts the field during the same time period drastically (>1 ppm).

This procedure was used to adjust and recontrol our MR-system for more than 1 year and revealed even small changes of the system with time (e.g., changes of the eddy current characteristics in relation to the He level in the dewar). The decay constant $k(t)$ and frequency $\gamma \Delta B_z(t)$ are not exactly, but empirically proportional to the residual field influences, which is sufficient for the interactive optimization of the pre-emphasis unit. Note that according to Eqs. [3] and [4], the analysis is not dependent on long-term fluctuations of signal amplification. This allowed us to compare data from different sessions directly, even after coarse changes of the system (e.g., transmitter power, coils). The stability of the calculated signals was

such that subsequent experiments were identical within a few percent of the signal amplitude.

The images obtained with the sequence of Fig. 2 show a clear spatial and temporal variation of the eddy current-generated fields (Fig. 3). The sequence is, however, time consuming and thus able to characterize a system, but not suitable for interactive and iterative adjustments. The particular gradient sequence as well as the imaging plane can be chosen arbitrarily. A time-course as shown in Fig. 3 can be obtained by a series of experiments with increasing t_a. The data in Fig. 3 demonstrate that the influence of the switched gradient diminishes with time, as expected, but is still present after

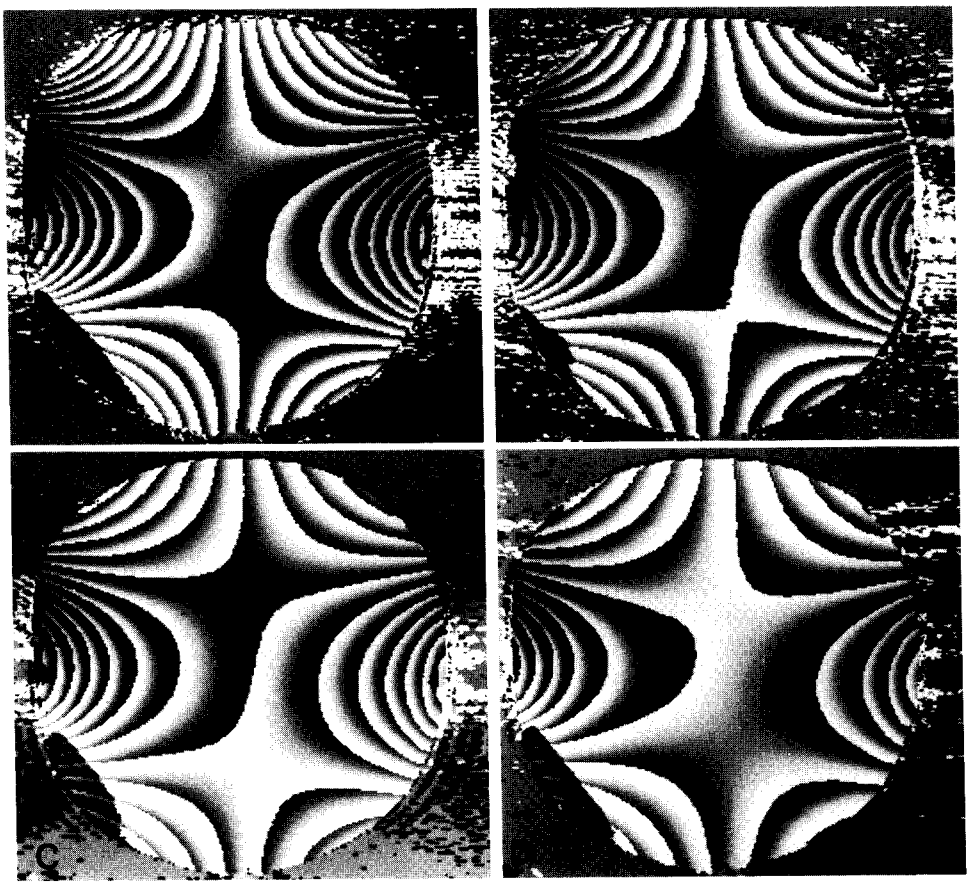

FIG. 3. Time-dependence and spatial distribution in a coronal (x, z) plane of eddy current-induced magnetic fields, measured by the imaging sequence in Fig. 2. The first pulse was (A) t_a = 5 ms, (B) t_a = 20 ms, (C) t_a = 50 ms, and (D) t_a = 100 ms after switching off a stationary x gradient (6.3 mT/m). Phase discontinuities appear due to phase wrapping and indicate isolines of eddy current fields, similar to a contour plot. From TE/2 = 15 ms, Eq. [6] provides a calculation of a frequency difference of 66 Hz between two discontinuities.

100 ms. The volume, where residual eddy current-induced field changes are acceptable, increases with time and can be determined with this method.

Improvement of Eddy Current Performance by Gradient Pre-pulses

One possible way of reducing eddy current-induced errors of the field is to add inverted gradient pulses in an ineffective time period just before the operative gradient, i.e., to add "gradient pre-pulses" affecting only the eddy current behavior of the system during the acquisition period as it is shown in Fig. 4 for an ISIS sequence (*4*).

In Figs. 5 and 6, the improvement of the eddy current performance of the modified ISIS sequence is monitored by the suggested FID analysis (Eq. [4]) and the imaging sequence (Fig. 2), respectively. The calculated decay $k(t)$ as well as the corresponding spectrum show the degradation of the quality of the magnetic field after gradient switching (Fig. 5). However, the line shape is restored using gradient prepulses. The sequence also demonstrates the sensitivity of the time-resolved decay analysis $k(t)$ to changes of the magnetic field quality.

In Fig. 6, the same gradient prepulse scheme of Fig. 4 is characterized by the imaging sequence of Fig. 2. The increased distances between the phase discontinuities (corresponding to approximately 0.1 ppm field changes) in the corrected sequence (Fig. 4B) show that the volume available for spectroscopy increases dramatically. The last gradient is switched off 20 ms before the 90° pulse of the eddy current imaging sequence. For the performance of the ISIS sequence in the outer parts of the images in Fig. 6, one has to consider displacement of the localized volume as well as line broadening.

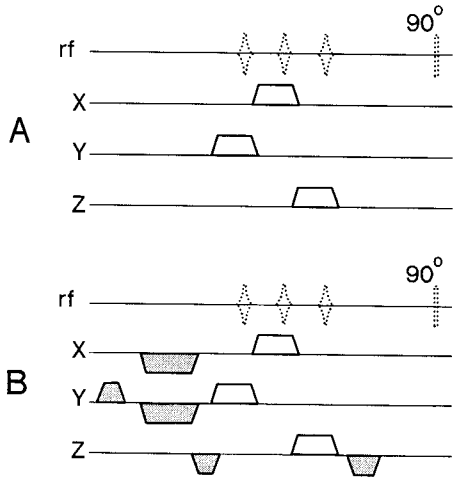

FIG. 4. The ISIS sequence (*4*) was modified with gradient prepulses to reduce eddy current effects. (A) Sequence without and (B) with additional gradient prepulses. The standard gradient pulses necessary for the localization experiment are unshaded. Note that the compensated sequence has a shorter time interval between the last gradient action and the acquisition (stabilization delay). The radiofrequency pulses of the ISIS experiment are indicated by dashed lines for timing purposes (65, 50, and 35 ms prior to the 90° pulse) but were not applied in the experiments presented here. The delay in (B) between the last gradient switching (z gradient) and the 90° pulse was 20 ms.

Quantitative Analysis of an Image Series by Means of Inhomogeneity Terms

Figures 3 and 6A prove that the residual eddy current-induced fields after pre-emphasis adjustment cannot be described simply by linear gradients and shifts of the main field only. The angular dependence of the phase-discontinuities indicates that terms in Eqs. [7]–[9] with higher values of m are present even hundreds of milliseconds after switching off the x gradient.

For a numerical analysis in all three dimensions, a series of tilted image planes was chosen. This allowed the determination the eddy current field on-axis and on 7 rings perpendicular to the z axis, respectively. The analysis revealed a strong z dependence of the eddy current fields after switching off the x gradient (Fig. 7A). To control the measurements of the off-axis eddy current effects, we determined the field additionally in a transversal slice at $z = 0$ (perpendicular to the z axis and to the tilted slices). In Fig. 7B, magnetic fields measured in the transversal plane are compared with those obtained from identical locations in the tilted slices, proving that the measurements are nearly independent of the orientation of the slice.

A low gradient strength of 3 mT/m was selected to avoid too many phase-discontinuities, which complicates the read-out of the data. An increase of the gradient strength would obviously increase the eddy current effects.

The results of a numerical analysis of the residual magnetic fields are given in Table 2, according to Ref. (*8*). The impression gained from Fig. 7 is confirmed in Table 2: not only the term A_{11} (corresponding to the x gradient) is non-zero, but also the terms C_1 and B_{11} (corresponding to the other gradients z and y), and higher terms, e.g., A_{31}

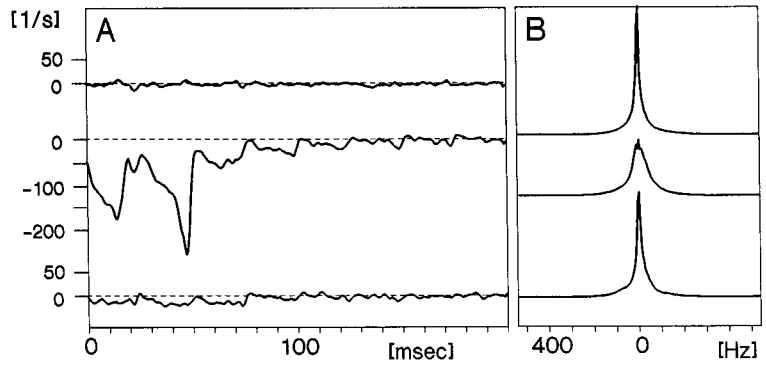

FIG. 5. Improvement of gradient switching sequences by gradient prepulses on a 12-cm water phantom. (A) Effects of the modification of an ISIS sequence on the suggested $k(t)$ analysis (*4*). The corresponding pulse-and-acquire spectra (B) with the same acquisition time (200 ms) justify the changes observed by the $k(t)$ analysis in (A). The spectra show—within a few Hz—the same frequency shift. The time-dependent $\gamma\Delta B_z(t)$ shift (not shown) and the $k(t)$-dephasing (A) result in a broadening of the spectra. Upper trace: without gradient switching (baseline, reference spectrum). Middle trace: ISIS gradient sequence without gradient prepulses (Fig. 4A). Lower trace: Modified ISIS gradient sequence with additional gradient prepulses according to Fig. 4B. FID decays are referenced to decays where no switching was performed. The top trace of A is also referenced to an (identical) experiment obtained without gradient switching, thus illustrating the reproducibility of the analysis. Note that the signals are not acquired by the ISIS sequence itself but that only the eddy current effects of the ISIS sequence are tested.

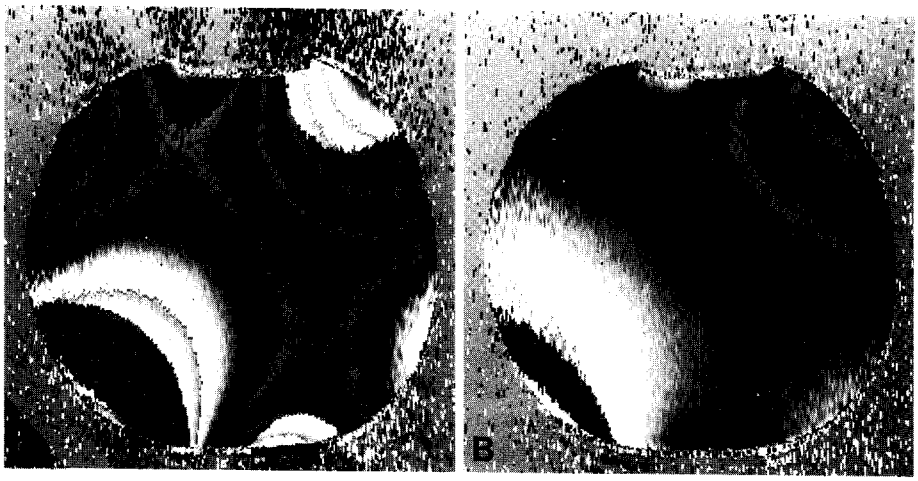

FIG. 6. Spatial distribution of fields induced by eddy currents generated from the gradient pulse train of an ISIS sequence (*8*) according to Fig. 4. The sagittal field maps have been produced by the imaging sequence described in Fig. 2 at the time when the ISIS readout pulse would be applied. Phase discontinuities have been enhanced in both images by the modulo function and correspond to approximately 0.1 ppm. (A) Field distribution after the gradient train of the uncompensated ISIS sequence shown in Fig. 4A. (B) The optimized sequence of Fig. 4B shows drastically reduced field variations. Therefore, the volume with acceptable effects on volume localization and linewidth is increased.

are present. An important difference between coefficients and maximal values can be seen by comparing Table 2A and Table 2B: The coefficient of the x gradient is the most prominent in Table 2A. However, due to the r^n dependence of the magnetic field (Eqs. [7]–[9]), inhomogeneities with a higher value of n become progressively important in larger volumes. This is illustrated in Table 2B where the maximum values of the magnetic field caused by the different spherical harmonics are calculated on a sphere with an 8-cm radius. Remote from the center of the magnet, nonlinear terms (e.g., A_{31}) become predominant. This is in agreement with experimental evidence, showing that excellent spectroscopic data can be acquired near the center of the magnet but not in a larger volume.

For imaging applications, it is important to realize that the A_{31} inhomogeneity of 439 Hz in Table 2B already causes a considerable spatial misregistration of four pixels (spectral width 25,000 Hz, 256 × 256 pixels matrix size), which increases with larger gradient strength or with a shorter delay between switching and data acquistion.

DISCUSSION

In this article, we presented two methods for the optimization and characterization of the eddy current behavior of an MR system and of pulse sequences:

(A) After gradient switching, the acquisition of a series of FIDs from an extended sample and a subsequent analysis of each pair of data points allow a separate and on-line observation of zero- and higher-order temporal fluctuations of the magnetic field.

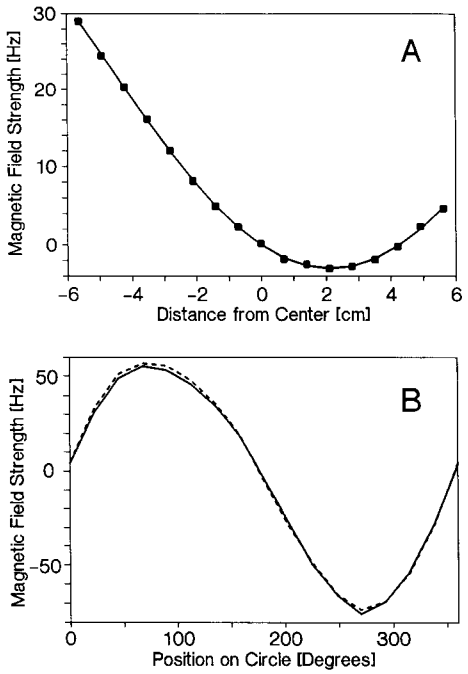

FIG. 7. Quantitative representation of influences from eddy currents 20 ms after a 3 mT/m x gradient pulse of 2500 ms duration. (A) Eddy current field distribution along the z axis (magnet axis). The points indicate the measured field "on-axis" as an average of nine different slice-orientations. The solid line represents the analysis according to Eq. [9] and Table 2 and shows clearly the strong z and z^2 components. (B) Comparison of the influence of eddy currents determined in different slice orientations. The solid line represents the measurements of the eddy current fields on a circle lying in a transversal slice. The broken line was observed at the same positions, but in slices which were tilted successively by 22.5° around the z axis. The excellent agreement illustrates the reliability of the obtained results with respect to the slice orientation. The magnetic field in all slices was set to zero at the magnetic center

In contrast to the determination of eddy current effects with the signal from two microprobes, an extended volume reveals all higher-order inhomogeneities. This method (Eqs. [3] and [4], Fig. 1) was used for an interactive adjustment of the pre-emphasis unit of our magnet prior to all further experiments. The analysis of the FID is not dependent on long-term fluctuations of the signal amplification, thus favoring its application in computer-controlled iterative algorithms, which can be sensitive to such changes of the signal. With an acquisition period matched to the length of the FID, the accuracy of the analysis seems to be limited less by statistical noise than by systematic errors (e.g., residual xy magnetization from the former FID). The sensitivity of the analysis was sufficient to monitor residual eddy current effects after careful adjustment of the pre-emphasis unit (Fig. 1).

When adjusting a pre-emphasis unit, one has to consider that the signal reflects all components of eddy currents, as seen in Table 2. In principle, the adjustment of the usually linear pre-emphasis corrections is thus influenced by higher order eddy currents,

a situation which is completely analogous to standard shim procedures, where one tries to compensate all orders of inhomogeneities with a few shim coils.

Another application of the proposed FID-method clearly proves that gradient pulse trains can be optimized by adding "dummy" gradient prepulses solely for the reduction of eddy current effects in the acquisition window (Fig. 5). Comparing analysis and spectrum after the compensated ISIS sequence in Fig. 5, one can estimate the sensitivity of the method: The spectrum shows residual broadening compared to the spectrum without any gradient switched. This slight difference is also visible in the analysis. The accuracy of the method can be estimated from the top trace, where the difference of two curves is shown, both without gradient switching.

(B) The imaging sequence (Fig. 2) permits the characterization of the temporal and spatial fluctuations of the magnetic field after any gradient switching sequence. The images contain information about the extension of the volume, in which distortion-free imaging and spectroscopy data can be obtained, after careful adjustments of pre-emphasis and gradient sequences have been done. The proposed imaging sequence proves also the efficiency of the implementation of "dummy" gradient prepulses (Fig. 4B) and allows to estimate the increased volume, available for spectroscopy after the improvement (Fig. 6). It clearly shows the residual distortions in the outer regions, which can cause line broadening and spatial misregistration in a ISIS sequence. Opposite switching of a gradient within a short time period (typically milliseconds) tends to cancel the resulting eddy current effects, at least those with a slower decay. This mechanism could explain the effect of gradient prepulses as well as the general observation that stationary gradients (>2 s) show much stronger eddy current effects than short gradient pulses (<10 ms) of the same gradient strength.

Quantitative analysis of the data obtained with the suggested imaging sequence of Fig. 2 clearly proves that gradient-induced eddy-current fields in a real, slightly asymmetrical magnet show terms of nonlinear behavior, i.e., terms of higher degree and order in the harmonic description of the magnetic field: B_0 shifts as well as highly nonlinear eddy current fields. The coefficients A_{nm}, B_{nm}, and C_n (Table 2A) are essential for the calculation of field distortions. Nevertheless, the maximum values of the field within a sample are much more significant for the determination of the influence on the inhomogeneity (Table 2B). Compared to the coefficient, terms with higher values of n are much more pronounced in the maximum values due to their r^n-dependence. One has also to consider that the listed values in Table 2 are obtained with a gradient-strength of only 30% of the maximum value and 20 ms after switching, whereas some phase encoding chemical-shift imaging sequences would require a waiting period of less than 1 ms between turning off the gradient and start of the acquisition. For a complete correction of these fields even for stronger gradients and shorter time delays, it would be necessary to add correction currents in much more than just the linear shim coils. With an increasing number of coils (each with at least three amplitudes and three time constants), such a correction becomes increasingly difficult, if not impossible, in such magnets as the one used here, even if an analytical determination of the eddy currents (*9, 10*) is used. Thus, we conclude that a significant reduction of eddy currents by a combination of active shielded gradients (*3*) and an increased

distance between gradient tube and conducting parts of the magnet is mandatory. Only minor effects should be present thereafter. In addition, magnet technology should help to make these residual eddy currents highly symmetrical, with clearly defined time constants such that a compensation by a pre-emphasis unit is feasible. Postprocessing (*11, 12*) or the implementation of "dummy gradient pulses" (Fig. 4) may be helpful for the additional optimization of extremely sensitive experiments.

The accuracy of the quantitative analysis depends on two experimental parameters: (i) The number of points on the circles (16 in this experiment) define the largest m, which can be determined according to the sampling theorem. (ii) The number of planes (7 for this analysis) limits the highest value of n in the statistical evaluation.

The suggested imaging sequence and the numerical representation of the inhomogeneities allow a quantitative and transferable characterization of any magnet/gradient system and could be added to the data sheet of the technical specifications. They give a precise characterization of the available volume in an MR system and permit an objective measurement of technical improvements. The exact separation of the different gradients should be extremely helpful in finding structures which act as sources of eddy currents.

The imaging sequence and the quantitative analysis result are restricted by the finite length of the echo period TE/2 which produces a time-averaged value (Eq. [6]) and by the time τ separating the second and third pulse (Fig. 2). One has to distinguish two extreme cases: (i) Very fast eddy currents, which disappear within TE/2 (and $t_a = 0$), can be underestimated by the averaging. (ii) Very slow eddy currents, on the other hand, could reduce the net effect because they are still present after the time τ (approximately 1 s). The time scale of the imaging experiment in this article was chosen to characterize those eddy current fields which are significant during the acquisition period of the sequences mostly used on this system (i.e., spin-echo MRI and ISIS), and therefore, "fast" and "slow" eddy current fields are not evaluated. For other MR systems, the timing of the sequence could be adapted by shortening TE/2 and increasing τ (if necessary with degassed phantoms to increase T1).

The quantitative analysis can be extended by measurements at different time intervals t_a after gradient switching, thus giving a time course of the spatially resolved information.

CONCLUSIONS

The proposed FID analysis and imaging sequences are valuable tools for the basic analysis of magnet/gradient systems, for the adjustment of the pre-emphasis correction unit, and for the design of eddy current insensitive imaging or spectroscopy sequences.

An application of the suggested methods shows quantitatively that a compensation of eddy currents by pre-emphasis methods has its limitations in a real magnet because of the need to correct higher order terms which are still present after the adjustment of the pre-emphasis. This is not generally feasible and proves that effects of eddy currents have to be reduced instead of compensated by opposed currents in the shim coils.

ACKNOWLEDGMENTS

We thank E. Ungricht (Bruker-Spectrospin, Fällanden) for very helpful discussions about the magnetic field analysis. We acknowledge A. Nauerth and M. Hörmann (Bruker, Karlsruhe) for providing us with a powerful phase-image calculation package. The project was supported by grants from the Swiss National Science Foundation (3.941-0.84 and 4.894-0.85.18), the Committee for the Promotion of Applied Scientific Research, the Kamillo-Eisner-Stiftung and Spectrospin AG.

REFERENCES

1. P. MANSFIELD AND P. G. MORRIS, "NMR Imaging in Biomedicine," Academic Press, New York, 1982.
2. R. E. GORDON AND W. E. TIMMS, *Comput. Radiol.* **8,** 245 (1984).
3. P. MANSFIELD AND B. CHAPMAN, *J. Magn. Reson.* **66,** 573 (1986).
4. R. J. ORDIDGE, A. CONNELLY, AND J. A. B. LOHMAN, *J. Magn. Reson.* **66,** 283 (1986).
5. C. BOESCH AND E. MARTIN, *Radiology* **168,** 481 (1988).
6. C. BOESCH AND E. MARTIN, *Magn. Reson. Med.* **15,** 357 (1990).
7. A. G. REDFIELD AND S. D. KUNZ, *J. Magn. Reson.* **19,** 250 (1975).
8. F. ROMEO AND D. I. HOULT, *Magn. Reson. Med.* **1,** 44 (1984).
9. J. J. VAN VAALS, "Proceedings of the 8th Annual Meeting of the Society Magnetic Resonance in Medicine, Amsterdam" Vol. 1, p. 183, Soc. Magn. Reson. Med., Berkeley, 1989.
10. P. JEHENSON, M. WESTPHAL, AND N. SCHUFF, "Proceedings of the 8th Annual Meeting of the Society Magnetic Resonance in Medicine, Amsterdam" Vol. 2, p. 966, Soc. Magn. Reson. Med., Berkeley, 1989.
11. R. J. ORDIDGE AND I. D. CRESSHULL, *J. Magn. Reson.* **69,** 151 (1986).
12. P. JEHENSON AND A. SYROTA, *Magn. Reson. Med.* **12,** 253 (1989).